ISSN: 3064-6758 www.aristonpubs.com/sciengg-advances https://doi.org/10.69626/sea.2024.0124

RESEARCH ARTICLE

# Fabrication and Characterization of Silicon Quantum Dots Thin Films for Optoelectronic Applications

**Aditya Srivastava, Shamshad A. Khan, Archana Srivastava***

**ABSTRACT:** Silicon quantum dots (Si-QDs) have garnered significant attention due to their tunable optical and electronic properties, making them ideal candidates for optoelectronic devices, including solar cells. In this study, we synthesized thin films of Si-QDs with a thickness of 20 nm on quartz substrates using a physical vapor deposition method under varying substrate temperatures (165 K, 135 K, and 115 K) and a constant argon gas pressure (4 Torr). The structural, optical, and electrical properties of the Si-QDs were extensively characterized to assess their potential in optoelectronics. X-ray diffraction (XRD) analysis revealed the amorphous nature of the synthesized quantum dots, with no sharp crystalline peaks detected, indicating nanoscale dimensions. Field Emission Scanning Electron Microscopy (FESEM) and High-Resolution Transmission Electron Microscopy (HRTEM) imaging confirmed quantum dot sizes ranging from 3-7 nm, with well-dispersed nanoparticles forming a uniform thin film. Optical properties were analyzed using UV-Visible spectroscopy, which demonstrated a distinct absorption edge corresponding to a direct band gap, suggesting strong quantum confinement effects in the Si-QDs. The optical band gap varied slightly depending on the deposition temperature, indicating temperature-dependent quantum dot size control. Electrical measurements were conducted through temperature-dependent DC conductivity (I-V-T) analysis, which revealed an exponential increase in conductivity with rising temperature, confirming the semiconducting behavior of Si-QDs. These results underscore the potential of Si-QDs as high-efficiency materials for optoelectronic devices, particularly in solar cell applications, due to their direct band gap, high absorption coefficient, and favorable electrical conductivity.

**Keywords:** Silicon Quantum Dots (Si-QDs), Optoelectronic Devices, Thin Films, Electrical Properties, DC Conductivity.

**Received: 03 June 2024; Revised: 25 July 2024; Accepted: 17 August 2024; Available Online: 29 August 2024**

## 1. INTRODUCTION

In the present nanotechnology world, Si is one of the most dominant material for optoelectronic devices. To fabricate functional devices, it is important to understand the electrical, optical, and other characteristics of Si quantum dots in detail. The Si quantum dots have unique properties, such as their use in new-generation solar cells [1, 2]. The synthesis of quantum dot Solar cells (QDSSCs) is easy and it has a wider band gap semiconductor electrode, sensitizer, counter electrode, and redox electrolyte [3]. These solar cells have fascinated researchers due to various advantages such as cheap production cost, tuned bandgap according to size because of the quantum confinement effect over traditional solar cells [4, 5]. Because of these reasons, the semiconductor QDs can enhance the power conversion efficiency of solar cells. Since quantum dots offer large optical band gaps and the band gap governs the absorption wavelength of quantum dots [6]. The highly efficient QDSSCs have a striking influence in the power generation field during this time of energy crisis. This will also reduces the emission of greenhouse gases [7]. The span of the collected solar spectrum will decide the conversion efficiency of solar cells. Generally, a huge portion of the solar spectrum is lost in the IR and UV ranges. In solar cell materials, the ultraviolet photons create hot electrons

Materials Science Research Lab, Department of Physics, St. Andrews College, Gorakhpur-273001, Uttar Pradesh, India

* Author to whom correspondence should be addressed: 31archana84@gmail.com (Archana Srivastava)

which are thermalized due to the coupling of phonons. These thermalized electrons do not constitute current. Due to these electrons, the temperature of solar material increases as well as efficiency decreases. Among various inorganic materials studied for solar cells so far, the use of Silicon quantum dots is of utmost importance and increases the power conversion efficiency [8]. The Silicon quantum dots are the perfect nanomaterial for solar cell usage with proven quantum characteristics and properties [9, 10]. The Si quantum dots are stable besides soaking of light and high absorption constant in comparison to other forms of Silicon. So, due to these unique and extraordinary properties, Si quantum dots are chosen by the researchers for the exploration about the best candidate as the solar cell material. Researchers are hopeful about pavement of striking and new path in the Si based advanced solar cell technology.

One can easily control the physical properties of nanomaterial by adjusting size of the particle. The semiconductor quantum dots (QDs) consists quantum confinement effect and got widespread attention due to their contemporary technical and scientific uses [11]. These quantum dots are assuring candidates due to their outstanding optical and electrical parameters which can be easily optimized based on choice of required device [12]. In recent years, it has been found that Si nanostructures are applicable in several advanced usage such as nano-electronic and opto-electronic devices [13, 14]. The workers also tend towards the exploration about luminescence properties of Si quantum dots and also noticed about the effect on the optical properties of Si QD's by quantum confinement [15, 16].

Significant research has been conducted on Si quantum dots for enhancing solar cell efficiency. Noteworthy works include studies on improved solar cell efficiency using Si quantum dots by Hong-Chen et al. [17], surface modification of Si quantum dot-sensitized solar cells by Hyunwoong Seo et al. [18], and investigations on Si quantum dots by Anna Castaldo et al. [19]. Further, Hyunwoong Seo et al. [20] explored the effect of different compositions on the performance of Si quantum solar cells, while Marc Rüdiger [21] studied bifacial n-type silicon solar cells. Research on Si tandem solar cells by H. Heidarzadeh et al. [22], the photoresponse of silicon quantum dot nanostructures in Si-rich nitride films by Pei Ling Li et al. [23], and Si quantum dot structures and their applications by L. Shcherbyna et al. [24] also contribute valuable insights. Other notable works include studies on the structural and electroluminescent properties of Si quantum dots by Yunjun Rui et al. [25], theoretical modeling of thin-film silicon solar cells by Zeman et al. [26] and analysis of hydrogenated amorphous silicon solar cells by Rodríguez et al. [27]. Dietmar Kohler et al. [28] analyzed large defect clusters in multicrystalline Si solar cells, while Tripathi et al. [29] investigated amorphous and nanocrystalline Si films deposited via the filtered vacuum arc technique. Zhang et al. [30] studied colloidal Si quantum dots for high-efficiency photovoltaics, and Gu et al. [31] have examined the properties of phosphorus-boron co-doped Si quantum dots thin film. Sofronov et al. [32] focused on photoinduced mid-infrared interband light absorption and photoconductivity in Ge/Si quantum dots, and Das and Sarkar [33] worked on Si nanowires for implications in heterojunction solar cells. Spruijtenburg et al. [34] have provided a fabrication guide for planar Si quantum dot heterostructures.

The current research focuses on the synthesis, as well as the structural, optical, and electrical characterization of Si quantum dots, fabricated at varying substrate temperatures at a constant ambient argon pressure.

## 2. EXPERIMENTAL DETAILS

### 2.1. Fabrication of Silicon quantum dots (Si-QDs) thin films

Silicon quantum dots (Si-QDs) thin films, with a uniform thickness of approximately 20 nm, were synthesized on quartz substrates using the Physical Vapor Deposition (PVD) method. Silicon chips served as the source material and were placed in a graphite crucible positioned within a vacuum chamber. The chamber was evacuated to a high vacuum level of $10^{-6}$ Torr using a turbo molecular pump to eliminate any contaminants. Subsequently, argon (Ar) gas was introduced into the chamber, maintaining a working pressure of 4 Torr. The substrate temperatures were regulated at three distinct levels—165 K, 135 K, and 115 K—using liquid nitrogen cooling to control the size and deposition rate of the Si-QDs. Once the deposition process was complete, thin films of Si-QDs with varying dot sizes were successfully formed on the quartz substrates. The thickness of the films was accurately measured using an Edward FTM-7 quartz crystal thickness monitor.

### 2.2. Structural Analysis

The amorphous nature of the synthesized Si-QDs was confirmed through X-ray diffraction (XRD) analysis performed with a Rigaku Ultima IV High-Resolution X-Ray Diffractometer (HRXRD), utilizing a copper (Cu) target as the radiation source with a wavelength of λ=1.54056A˚ (Cu-Kα1). The scan range for XRD measurements spanned from 30° to 70°, with a scanning rate of 2° per minute, providing critical insight into the structural characteristics of the Si-QDs.

### 2.3. Morphological Studies

Field Emission Scanning Electron Microscopy (FESEM) and High-Resolution Transmission Electron Microscopy (HRTEM) were employed to investigate the surface morphology and size distribution of the quantum dots. These imaging techniques offered high-resolution visualizations, confirming the uniformity and nanoscale dimensions of the Si-QDs, which ranged between 3-7 nm in size, depending on

 

the substrate temperature.

### 2.4. Optical and Electrical Measurements:

The optical properties of the Si-QDs thin films were characterized using LAMBDA 365 UV-Visible spectroscopy. Absorption spectra were recorded to determine the optical band gap and evaluate the quantum confinement effects in the synthesized Si-QDs. For electrical conductivity measurements, silver paste was applied as a contact electrode on the thin films. The films were mounted onto a specialized metallic sample holder, where a high vacuum of $10^{-4}$ Torr was maintained during the measurements. Temperature-dependent DC conductivity was assessed using a Keithley Model-617 digital electrometer. The experimental setup involved a constant voltage applied across the thin films, while the current response was recorded as the temperature of the sample was incrementally increased from 308 K to 428 K in steps of 5 K. This systematic temperature variation allowed for the examination of the thermal activation energy and semiconducting behavior of the Si-QDs thin films.

## 3. RESULTS AND DISCUSSION

**FESEM Studies:** The surface morphology of silicon quantum dots (Si-QDs) synthesized at varying substrate temperatures of 165 K, 135 K, and 115 K under a constant argon pressure of 4 Torr was investigated using Field Emission Scanning Electron Microscopy (FESEM). Figures 1 (a-b-c) present the FESEM images of Si-QDs deposited at these temperatures. It is observed that the quantum dots exhibit a spherical shape with an average size of approximately 5 nm. Notably, as the substrate temperature decreases, the size of the Si-QDs remains within a similar range, but there is a slight tendency for increased aggregation at higher temperatures. This aggregation suggests that the thermal energy available at higher temperatures facilitates a greater degree of surface diffusion and coalescence of quantum dots, leading to clustering.

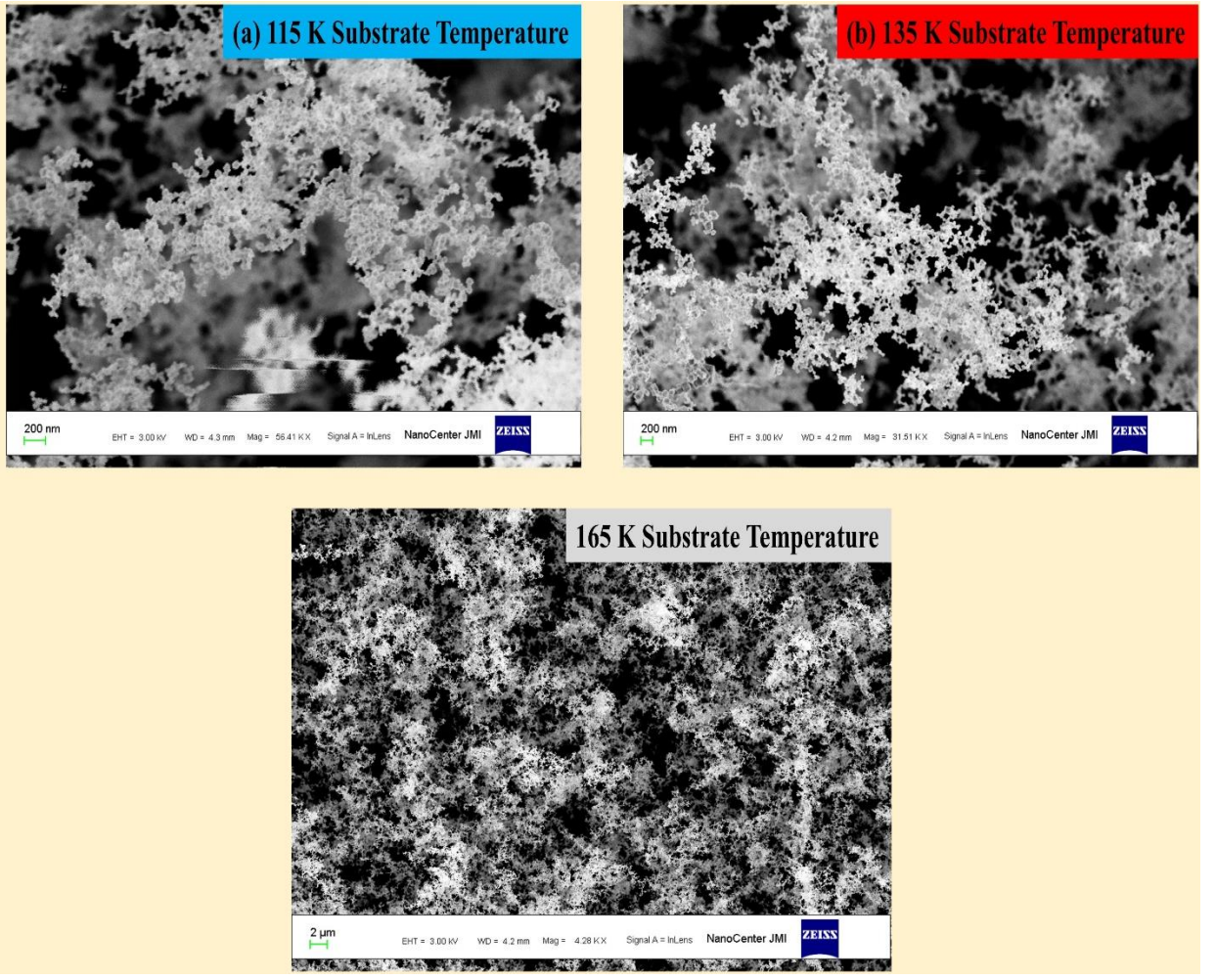


**Fig. 1.** (a-c): FESEM images of Si quantum dots prepared at substrate temperatures of 115 K, 135 K, and 165 K under 4 Torr Argon pressure.

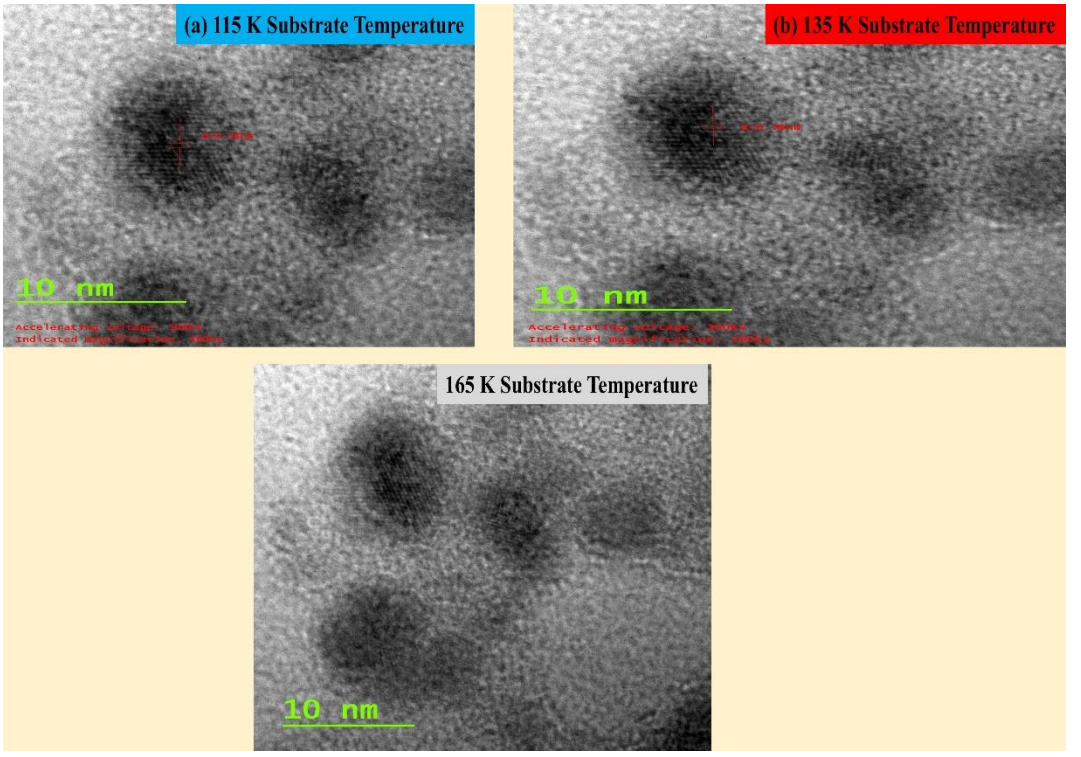


**Fig. 2.** (a-c): HRTEM images of Si quantum dots prepared at substrate temperatures of 115 K, 135 K, and 165 K under 4 Torr Argon pressure.

**HRTEM Analysis:** High-Resolution Transmission Electron Microscopy (HRTEM) images, displayed in Figures 2 (a-b-c), offer a more detailed examination of the size and arrangement of the Si-QDs synthesized at different substrate temperatures. The HRTEM results further corroborate the size range of the quantum dots, which varies between 3 to 7 nm. These nanodots are clearly distinguished in the images, though a degree of aggregation is visible, especially at higher substrate temperatures. This phenomenon could be attributed to the increased mobility of silicon atoms on the substrate surface at elevated temperatures, resulting in enhanced nucleation and growth of the quantum dots. The interparticle spacing of the Si-QDs, measured using HRTEM, reveals an average spacing of 0.36 nm for quantum dots deposited at 165 K, while the interspacing slightly increases to 0.37 nm for samples deposited at 135 K and 115 K. The increase in spacing at lower temperatures might suggest limited atomic mobility, preventing the coalescence of quantum dots and leading to a more isolated arrangement.

**X-Ray Diffraction (XRD) Studies:** The crystallographic structure of the Si-QDs was examined using X-ray diffraction (XRD), and the corresponding patterns are presented in Figure 3. The XRD analysis shows no distinct peaks for the quantum dots synthesized at any of the three substrate temperatures (165 K, 135 K, and 115 K), confirming their amorphous nature. The absence of crystalline peaks indicates that the Si-QDs did not exhibit long-range atomic order, which is typical for materials prepared at low temperatures via physical vapor deposition (PVD). The amorphous structure is advantageous for optoelectronic applications, as it can result in unique electronic properties that differ from their bulk crystalline counterparts, such as a direct bandgap in nanostructures.

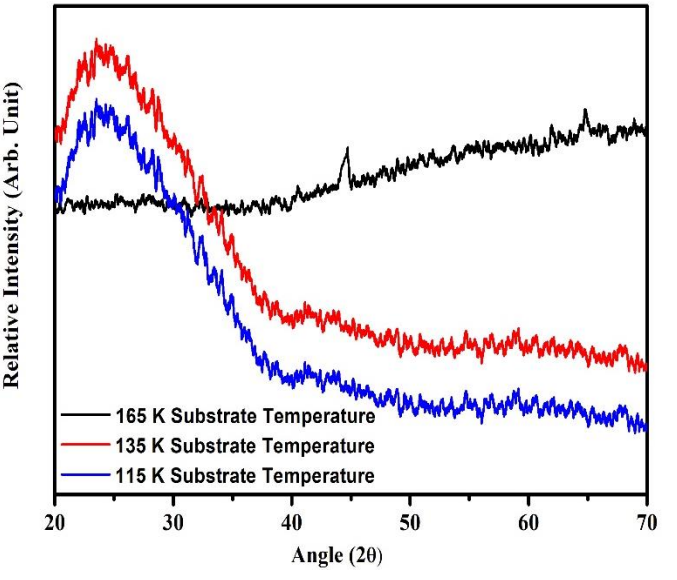


**Fig. 3.** HRXRD patterns of Si quantum dots prepared at substrate temperatures of 115 K, 135 K, and 165 K under 4 Torr Argon pressure.

 

**Optical studies:** Optical parameters of synthesized Silicon quantum dots at different substrate temperatures 165 K, 135 K and 115 K with fixed working pressure of 4 Torr have been determined within the wavelength span 400-900 nm. The optical density determined by UV-VIS spectrophotometer can be used to derive absorption coefficient (α) using the relation [35, 36].

$$\alpha = \text{Optical Density}/\text{ Film Thickness} \quad (1)$$

We have calculated α (absorption coefficient) using the above equation and shown in Figure 4. It was observed that absorption increases exponentially with the rise in photon energy for all thin films. The quantum dots fabricated at a higher substrate temperature (165 K) exhibit greater absorption than those prepared at a lower substrate temperature (115 K and 135 K), which can be attributed to the more aggression of quantum dots at higher substrate temperature. To calculate the optical band gap of a material, the following relation is used:

$$(\alpha h\nu)^{1/n} = B\,(h\nu - E_g) \quad (2)$$

where ν is the frequency of the incident beam, B is a constant, $E_g$ is the optical band gap, and 1/n is an exponent. The value of 1/n can be taken as 1/2, 3/2, 2, or 3, depending on the electronic transitions responsible for absorption [37, 38]. The system of Silicon quantum dots follows the direct transition rule, where the extrema lie at the same point in k-space [39]. Based on this direct transition, the equation is rewritten as:

$$(\alpha h\nu)^2 \propto (h\nu - E_g) \quad (3)$$

The relationship between $(\alpha h\nu)^2$ and photon energy (hν) for Silicon quantum dots is shown in Figure 5. The energy gap values were calculated by determining the X-axis intercept of the $(\alpha h\nu)^2$ *vs* (hν) plots. The calculated ($E_g$) values are presented in Table 1. The estimated optical band gap for quantum dots prepared at 115 K 135 K and 165 K substrate temperatures are 3.10 eV, 3.32 eV, and 3.52 eV respectively. This increment in the optical band gap with increasing substrate temperatures is due to the increase in the quantum dot size, as confirmed by the FESEM and HRTEM micrographs.

The "density of states model" proposed by Mott and Davis appears to be the most appropriate method for explaining the observed increase in bandgap, as optical absorption is directly influenced by short-range orderings and defects associated with non-crystalline states [40]. According to this model, the disorders and defects in non-crystalline structures are determined by the extent of localized states near the mobility edges. The variation in bandgap can also be attributed to shifts in the Fermi level, which are linked to the distribution of electrons in localized states [41]. The slopes of the straight line plots provide Tauc's parameter ($B^2$), which is strongly affected by the nature of bonding. The increase in $B^2$ with rising substrate temperature suggests that, at higher substrate temperature, the chemical ordering in the synthesized quantum dots is more organized [42].

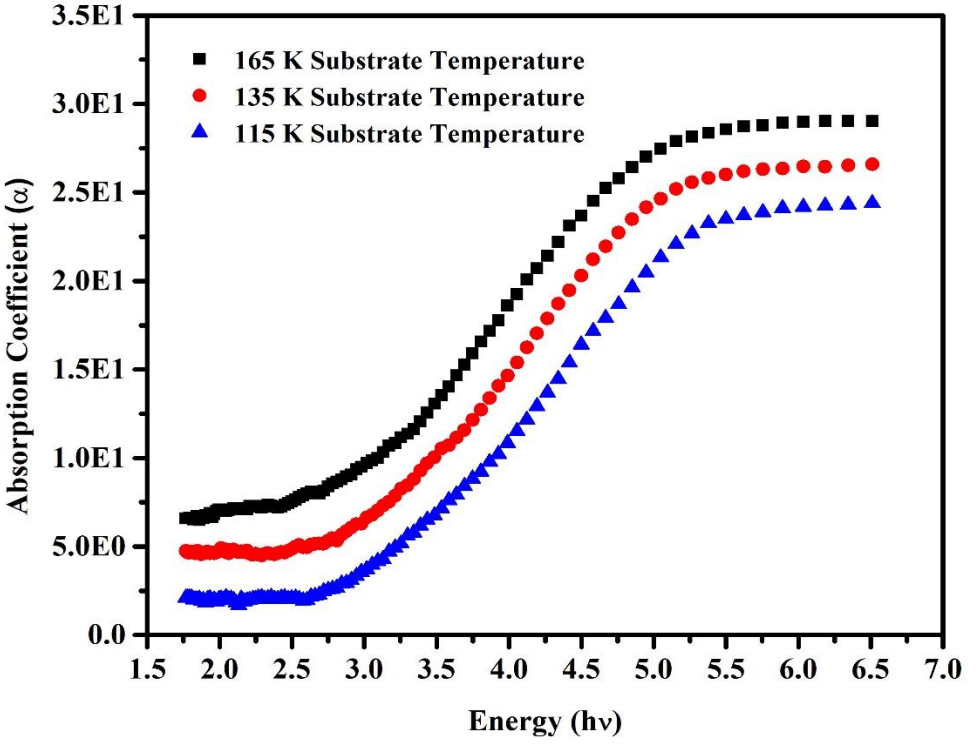


**Fig. 4.** Absorption coefficient as a function of energy for Si quantum dots prepared at substrate temperatures of 115 K, 135 K, and 165 K under 4 Torr Argon pressure.

**Table 1.** Optical and electrical parameters of synthesized Si quantum dots at different substrate temperatures under a constant Argon pressure of 4 Torr.

| S. No. | Substrate temperature (K) | Absorption Coefficient ($cm^{-1}$) at λ= 260 nm | Tauc's parameter ($B^2$) | Optical Band Gap Eg (eV) | $\sigma_{DC}$ ($\Omega^{-1}cm^{-1}$) at T=368 K | $\Delta E_c$ (eV) |
|---|---|---|---|---|---|---|
| **1.** | 165 | $24.83 \times 10^4$ | 1.34 | 3.52 | $6.45 \times 10^{-6}$ | 0.45 |
| **2.** | 135 | $21.72 \times 10^4$ | 0.86 | 3.32 | $4.42 \times 10^{-6}$ | 0.43 |
| **3.** | 115 | $19.68 \times 10^4$ | 0.57 | 3.10 | $2.96 \times 10^{-6}$ | 0.40 |

**Electrical studies:** The study of transport phenomena in synthesized Silicon quantum dots can be effectively carried out through electrical transport studies [43]. Analyzing the electrical transport properties of a material is particularly important, as it provides a straightforward way to understand certain physical characteristics of the synthesized sample [44]. The dark conductivity ($\sigma_{DC}$) of Si quantum dots at different temperatures (T) can be determined using the Arrhenius Equation [45].

$$\sigma_{DC} = \sigma_0 \exp(-\Delta E_c / KT) \quad (4)$$

This equation can be written as:

$$\ln \sigma_{DC} = \ln \sigma_0 - (\Delta E_c / KT)$$

or, equivalently:

$$\ln \sigma_{DC} = -(\Delta E_c / 1000\ K)(1000/T) + \ln \sigma_0 \quad (5)$$

This indicates a linear relationship between $\ln \sigma_{DC}$ and 1000/T, with the slope of this line equal to ($\Delta E_c$ /1000 K). The activation energy ($\Delta E_c$) can be calculated using the relation:

$$\Delta E_c = 1000\ K \times \text{slope of straight line} \quad (6)$$

where K is Boltzmann's constant. DC conductivity measurements of the synthesized Si quantum dots at different substrate temperatures were performed within a temperature range of 298 K to 393 K (Figure 6).

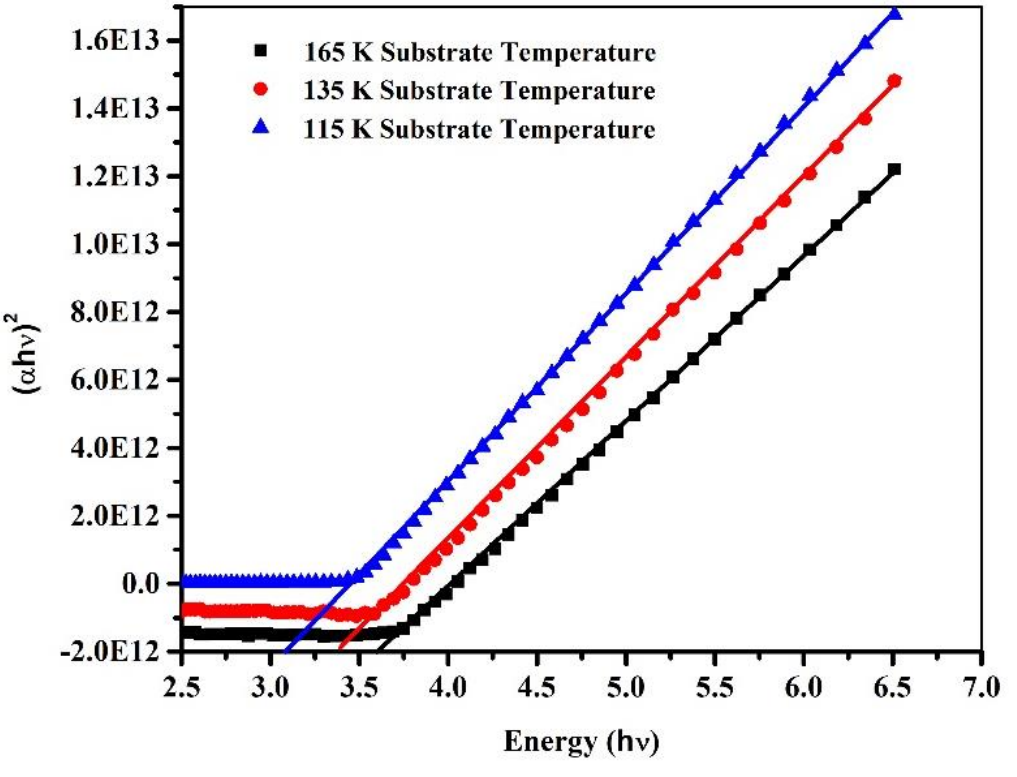


**Fig. 5.** $(\alpha h\nu)^2$ vs. hν (eV) for Si quantum dots prepared at substrate temperatures of 115 K, 135 K, and 165 K under 4 Torr Argon pressure.

 

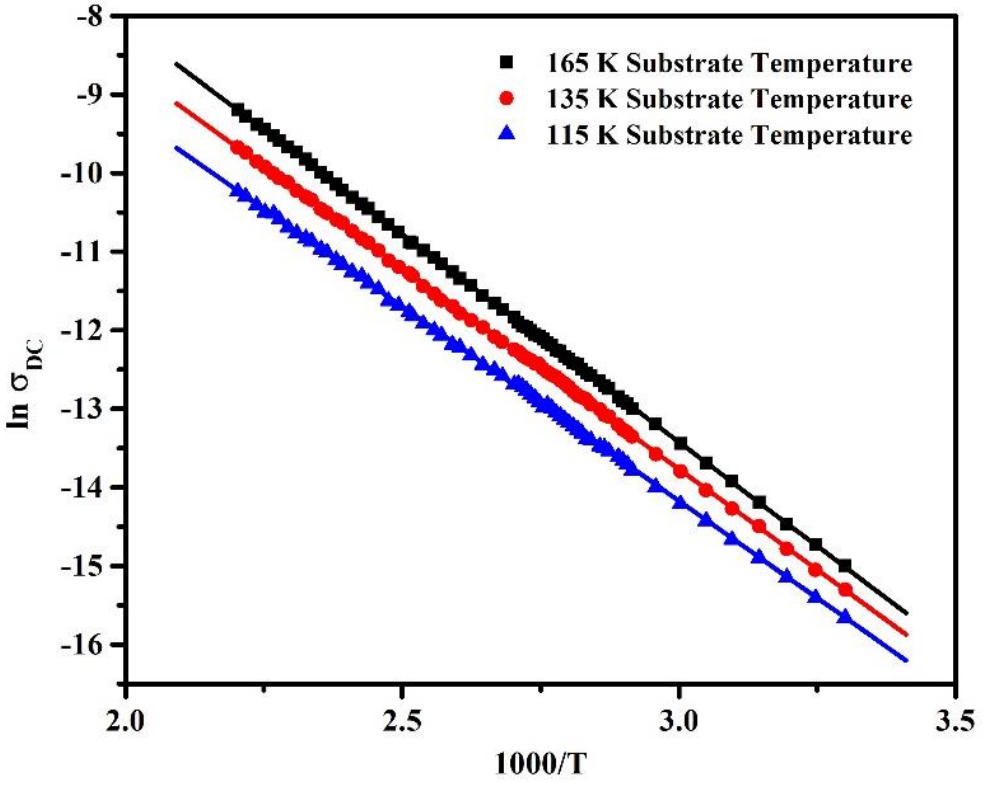


**Fig. 6.** Temperature dependence of dc conductivity in the range of 308 to 428 K for Si quantum dots prepared at substrate temperatures of 115 K, 135 K, and 165 K under 4 Torr Argon pressure.

The exponential increase in DC conductivity over this temperature range confirms the semiconducting nature of the prepared quantum dots. The estimated values of DC conductivity and activation energy at different substrate temperatures are listed in Table 1. The observed values suggest that the conduction mechanism in Si quantum dots is due to thermally-assisted charge carrier tunnelling within localized states of the band tails [46]. The slight increase in DC conductivity and activation energy with rising substrate temperatures can be attributed to a shift in the Fermi level [47] or an increased amount of hopping conduction via defect states [48].

## 4. CONCLUSION

In this study, we successfully synthesized and characterized silicon quantum dots (Si-QDs) with a focus on their structural, optical, and electrical properties. The morphological analysis via FESEM revealed the formation of Si-QDs with an average size ranging from 3 to 7 nm, a result corroborated by HRTEM imaging. These analyses confirmed the quantum confinement effects expected in such small nanostructures. The X-ray diffraction (XRD) studies further validated the amorphous nature of the Si-QDs synthesized at various substrate temperatures, which is a key characteristic for improving certain optoelectronic properties. The optical studies demonstrated a notable increase in the bandgap energy with decreasing quantum dot size, attributed to the quantum confinement effect. This tunability of the bandgap is essential for optimizing the absorption characteristics of Si-QDs in optoelectronic devices, such as solar cells, where efficient light harvesting is critical. The shift in the optical bandgap as a function of temperature indicates that substrate temperature during synthesis directly influences the quantum dot size and, consequently, their optical properties. In terms of electrical properties, the Si-QDs exhibited a typical semiconducting behavior, with the DC conductivity (σ DC) increasing exponentially as the temperature rose from 308 K to 428 K. This behavior suggests that charge transport in these materials occurs through an activated process, indicative of hopping conduction between localized states. The observed reduction in activation energy and the shift in the Fermi level at higher temperatures point to enhanced charge carrier mobility and a stronger percolation network in the more aggregated Si-QDs formed at elevated substrate temperatures. The findings from this research highlight the significant potential of Si-QDs for applications in optoelectronics, particularly in the field of solar energy conversion. The ability to control the size and aggregation of Si-QDs by varying substrate temperature allows for fine-tuning of both optical and electrical properties, making these materials promising candidates for the development of highly efficient, next-generation solar cells. Future work will focus on integrating these Si-QDs into device architectures and

exploring their performance under real-world conditions.

## CONFLICT OF INTEREST

The authors declare that there is no conflict of interests.

## ACKNOWLEDGEMENTS

The authors express their sincere gratitude to Prof. Zishan H. Khan, Department of Applied Science and Humanities, Faculty of Engineering and Technology, Jamia Millia Islamia, New Delhi, India, for providing access to experimental facilities in his research laboratory, as well as for his insightful discussions and valuable suggestions throughout the writing of this research paper.

## REFERENCES

[1] Morozova, S., Alikina, M., Vinogradov, A. and Pagliaro, M., **2020.** Silicon quantum dots: synthesis, encapsulation, and application in light-emitting diodes. *Frontiers in chemistry*, *8*, p.191.

[2] Terada S., Xin Y., and Saitow K., **2020.** Cost-Effective Synthesis of Silicon Quantum Dots. *Chemistry of Materials. 32* (19), pp.8382–8392.

[3] Singh S., Khan Z. H., Khan M. B., Kumar P., and Kumar P., **2022.** Quantum dots-sensitized solar cells: a review on strategic developments. *Bulletin of Materials Science.* 45(2), p. 81.

[4] Markna J. H. and Rathod P. K., **2022.** Review on the efficiency of quantum dot sensitized solar cell: Insights into photoanodes and QD sensitizers. *Dyes and Pigments. 199*, p. 110094.

[5] Sahu A., Garg A., and Dixit A., **2020.** A review on quantum dot sensitized solar cells: Past, present and future towards carrier multiplication with a possibility for higher efficiency. *Solar Energy*. *203* pp. 210–239.

[6] Rasal A. S., Yadav S., Kashale A. A., Altaee A., and Chang J.-Y, **2022.** Stability of quantum dot-sensitized solar cells: A review and prospects. *Nano Energy. 94*, p. 106854.

[7] Gressler S., Part F., Scherhaufer S, Obersteiner G., and Huber-Humer M., **2022.** Advanced materials for emerging photovoltaic systems – Environmental hotspots in the production and end-of-life phase of organic, dye-sensitized, perovskite, and quantum dots solar cells. *Sustainable Materials and Technologies. 34*, p. e00501.

[8] Cao Y., Zhu P., Li D., Zeng X., and Shan D., **2020.** Size-Dependent and Enhanced Photovoltaic Performance of Solar Cells Based on Si Quantum Dots. *Energies*. *13*(18).

[9] Alvi M. A., Al-Ghamdi A. A., and Khan S. A., **2018.** Characterization of Si quantum dots synthesized at various operating pressures for photovoltaic application. *Materials Research Express*. *5*(12) p. 125024.

[10] Al-Agel F. A., Suleiman J., and Khan S. A., **2017.** Studies on silicon quantum dots prepared at different working pressure. *Results in Physics. 7*, pp. 1128–1134.

[11] Khan Z. M. S. H., Khan H., and Zulfequar M., **2017.** CdSe quantum dots using selenourea as selenium source in polymer matrix. *Journal of Materials Science: Materials in Electronics. 28* (19), pp. 14638–14645.

[12] García de Arquer F. P., Talapin D. V, Klimov V. I., Arakawa Y., Bayer M., and Sargent E. H., **2024.** Semiconductor quantum dots: Technological progress and future challenges. *Science. 373(*6555), p. eaaz8541.

[13] Rai H., Singh K. R. B., Pandey S. S., and Natarajan A., **2024.** Role of Si and $SiO_2$ in Optoelectronic Device Fabrication. *Journal of Molecular Structure.1316*, p. 138994.

[14] Iqbal M. A., Nadia A., Maria M., Mohammed Al-B., Md. Rasidul I., Jeong Ryeol C., Phuong V. P., Xiaofeng L., **2023.** Nanostructures/Graphene/Silicon Junction-Based High-Performance Photodetection Systems: Progress, Challenges, and Future Trends. *Advanced Materials Interfaces. 10* (7), p. 2202208.

[15] Zhang Y., Cai N., and Chan V., **2023.** Recent Advances in Silicon Quantum Dot-Based Fluorescent Biosensors. *Biosensors. 13*(3).

[16] Zhang P., Li S. Li. D., **2023.** Quantum size-dependent luminescence and nonlinear optical properties of silicon quantum dots/SiO2 multilayer. *Optics and Laser Technology*. *157*, p. 108706.

[17] Hao H.-C., Shi W., Chen J.-R., and Lu M., **2014.** Mass production of Si quantum dots for commercial c-Si solar cell efficiency improvement. *Materials Letters*. *133*, pp. 80–82.

[18] Seo H., Wang Y., Uchida G., Kamataki K., Itagaki N., Koga K. and Shiratani M., **2013.** The reduction of charge recombination and performance enhancement by the surface modification of Si quantum dot-sensitized solar cell. *Electrochimca Acta*, *87*, pp. 213–217.

[19] Castaldo A., Antonaia A., and Addonizio M. L., **2014.** Synthesis of silicon quantum dots in zinc silicate matrix

 

by low-temperature process: Optical, structural and electrical characterization. *Thin Solid Films*, *562*, pp. 172–180.

[20] Seo H., Wang Y., Uchida G., Kamataki K., Itagaki N., Koga K. and Shiratani M., **2013.** Analysis on the effect of polysulfide electrolyte composition for higher performance of Si quantum dot-sensitized solar cells. *Electrochimca Acta*, *95*, pp. 43–47, 2013.

[21] Rüdiger M., Fischer S., Frank J., Ivaturi A., Richards B. S., Kramer K.W. Hermle M. and Goldschmidt J. C., **2014.** Bifacial n-type silicon solar cells for upconversion applications. *Solar Energy Materials and Solar Cells*, *128*, pp. 57–68.

[22] Heidarzadeh H., Baghban H., Rasooli H., Dolatyari M. and Rostami A., **2014.** A new proposal for Si tandem solar cell: Significant efficiency enhancement in 3C–SiC/Si. *Optik*, *125*(3), pp. 1292–1296.

[23] Li P. L, Gau C., and Liu C. W., **2013.** Correlation between photo response and nanostructures of silicon quantum dots in annealed Si-rich nitride films. *Thin Solid Films*, *529*, pp. 185–189.

[24] Shcherbyna L. and Torchynska T., **2013.** Si quantum dot structures and their applications. *Physica E: Low-dimensional Systems and Nanostructures*, *51*, pp. 65–70.

[25] Rui Y., Li S., Cao Y., Xu J., Li W. and Chen K., **2013.** Structural and electroluminescent properties of Si quantum dots/SiC multilayers. *Applied Surface Science*, *269*, pp. 37–40.

[26] Zeman M., Isabella O., Solntsev S., and Jäger K., **2013.** Modelling of thin-film silicon solar cells. *Solar Energy Materials and Solar Cells*, *119*, pp. 94–111.

[27] Rodríguez J. A., Fortes M., Alberte C., Vetter M., and Andreu J., **2013.** Development of a very fast spectral response measurement system for analysis of hydrogenated amorphous silicon solar cells and modules. *Materials Science Engineering: B, 178*(1), pp. 94–98.

[28] Kohler D., Zuschlag A. and Hahn G**., 2014.** On the origin and formation of large defect clusters in multicrystalline silicon solar cells. *Solar Energy Materials and Solar Cells*, *120*, pp. 275–281.

[29] Tripathi R. K., Panwar O. S., Rawal I., Singh B. P. and Yadav B. C.,**2018.** Study on nanocrystalline silicon thin films grown by the filtered cathodic vacuum arc technique using boron doped solid silicon for fast photo detectors. *Journal of Taiwan Institute of Chemical Engineers*, *86*, pp. 185–191.

[30] Zhang P., Feng Y., Wen X., Cao W., Anthony R. Kortshagen U., Conibeer G. and Huang S., **2016.** Generation of hot carrier population in colloidal silicon quantum dots for high-efficiency photovoltaics," *Solar Energy Materials and Solar Cells*, *145*, pp. 391–396.

[31] Gu Z., Shan F. and Liu J., **2024.** Properties of phosphorus-boron co-doped c-Si quantum dots/SiNx:H thin film prepared by PECVD in-situ deposition. *Scientific Reports.*, *14* (1), p. 21612.

[32] Sofronov A. N., Vorobjev L. E., Firsov D. A., Panevin V. Y., Balagula R. M., Werner P. and Tonkikh A. A., 2015. Photoinduced mid-infrared intraband light absorption and photoconductivity in Ge/Si quantum dots. *Superlattices Microstructures*, *87*, pp. 53–57.

[33] Das D. and Sarkar K., 2**024.** Growth Mechanism and Opto-Structural Characterization of Vertically Oriented Si Nanowires: Implications for Heterojunction Solar Cells. *ACS Applied Energy Materials*, *7*(15), pp. 6649–6666.

[34] Spruijtenburg P. C., Amitonov S. V., van der Wiel W. G. and Zwanenburg F. A., **2018.** A fabrication guide for planar silicon quantum dot heterostructures. *Nanotechnology*, *29* (14), p. 143001.

[35] Srivastava A., Khan Z. M. S. H., Khan Z. H., and Khan S. A., **2024.** Studies of $Se_{85}Te_{12}Bi_3$ and $Se_{85}Te_9Bi_6$ Nanochalcogenide Thin Films at Different Working Pressures. *Recent Advances in Nanomaterials*, pp. 133–140.

[36] Srivastava A., Akhtar M. S., Umar M., Hashem M., Alsarani M. M. Fouad H. and Khan S. A., **2023.** Comparative Study on Structural and Optical Properties of $Se_{85}Te_6Bi_9$ Nano-Thin Films Synthesized at Disparate Ambient Argon Pressures. *Science of Advanced Materials*, *15*(1), pp. 10–16.

[37] Srivastava A., Khan Z. H., and Khan S. A., **2024.** Effect of ambient argon pressure on the structural, optical and electrical properties of non-crystalline $Se_{85}Te_3Bi_{12}$ nano-thin films. *Journal of Physics D: Applied Physics*, *57*(9), p. 95303.

[38] Khan S. A., Sahani R. M., Tripathi R. P., Akhtar M. S., and Srivastava A., **2021.** Influence of gamma-irradiation on the optical and structural properties of Se85Te15-xBix nano-thin chalcogenide films. *Radiation Physics Chemistry*, *188*, p. 10965.

[39] Ryvkin S. M., **1965.** Indirect Optical Transitions Induced by Carrier Interaction in Semiconductors. *Physica Status Solidi (b)*, *11(*1), pp. 285–294.

[40] Wang Y. H., Lin J., and Huan C. H. A., **2003.** Structural and optical properties of a-Si:H/nc-Si:H thin films grown from $Ar–H_2–SiH_4$ mixture by plasma-enhanced chemical vapor deposition. *Materials Science Engineering: B*, *104*(1), pp. 80–87.

 

[41] Kumar A. and Ahluwalia P. K., **2012.** Electronic structure of transition metal dichalcogenides monolayers 1H-$MX_2$ (M = Mo, W; X = S, Se, Te) from ab-initio theory: new direct band gap semiconductors. *European Physics Journal B*, *85*(6), p. 186, 201.

[42] Parida A., Alagarasan D, Ganesan R., Bisoyi S., and Naik R, **2023.** Influence of time dependent laser-irradiation for tuning the linear–nonlinear optical response of quaternary $Ag_{10}In_{15}S_{15}Se_{60}$ films for optoelectronic applications. *RSC Advances*, *13*(7), pp. 4236–4248.

[43] Aslam Z., Rashid Lone Z., Shoab M., and Zulfequar M., **2023.** Investigation of electrical conduction and optical properties of amorphous Se88Zn10Bi2 chalcogenide thin film. *Chemical Physics Letters*, *814*, p. 140321.

[44] Al-Muntaser A. A., Abdelghany A. M., Abdelrazek E. M. and Elshahawy E. G., **2020.** Enhancement of optical and electrical properties of PVC/PMMA blend films doped with Li4Ti5O12 nanoparticles. *Journal of Materials Research Technology*, *9*(1), pp. 789–797.

[45] Meikhail M. S., Oraby A. H., El-Nahass M. M., Zeyada H. M., and Al-Muntaser A. A., **2018.** Electrical conduction mechanism and dielectric characterization of MnTPPCl thin films. *Physica B: Condensed Matter*, *539*, pp. 1–7.

[46] Wager J. F., **2017.** Real- and reciprocal-space attributes of band tail states. *AIP Advances*, *7*(12), p. 125321.

[47] Dan S., Chatterjee S. and Pal A.J, **2022.** Formation of $CuIn_{(1-x)}Ga_xS_2$ Thin Films through a Solution Approach: Nonlinear Variation of Fermi Energy and Band Gap Bowing. *Langmuir*, *38*(39), pp. 11909–11916.

[48] Pal S., Dalui T. K, and Basak D., **2023.** Unravelling the crossover amongst band and various hopping conduction mechanisms in Mo doped ZnO thin films owing to carrier localization at defects. *Journal of Alloys Compounds. 946*, p. 16933.

 